Journal of the European Ceramic Society 42 (2022) 3118–3126

Contents lists available at ScienceDirect

Journal of the European Ceramic Society

journal homepage: www.elsevier.com/locate/jeurceramsoc

Fabrication of B_4C ultrafiltration membranes on SiC supports

Cristina Ojalvo [a], María Jiménez-Fuentes [b], Wenjing Zhang [c], Fernando Guiberteau [a], Victor M. Candelario [b], Angel L. Ortiz [a,*]

[a] Departamento de Ingeniería Mecánica, Energética y de los Materiales, Universidad de Extremadura, 06006 Badajoz, Spain
[b] Department of Research and Development, LiqTech Ceramics A/S, Industriparken 22C, DK-2750 Ballerup, Denmark
[c] Department of Environmental Engineering, Technical University of Denmark, Miljøvej 113, Kgs., Lyngby 2800, Denmark

ARTICLE INFO

Keywords:
Ceramic membranes
Porous ceramics
B_4C
Ultrafiltration
Processing/sintering

ABSTRACT

The fabrication of B_4C ultrafiltration membranes is described. Firstly, a semi-dilute B_4C slurry was environmentally-friendly prepared by aqueous colloidal processing, optimizing its dispersion by sonication, and used to deposit B_4C membranes onto SiC macro-porous supports by dip-coating. Secondly, the resulting green membranes were characterised microstructurally by scanning electron microscopy (SEM), and pressureless sintered within the intermediate sintering regime. Thirdly, the sintered membranes were calcined in air to clean them from possible free carbon in the smallest pores, with the optimal calcination conditions having been identified by thermogravimetry coupled with mass spectrometry. Next, the calcined, sintered membranes were characterised microstructurally by SEM, tested mechanically against scratching, and characterised texturally by capillary flow porometry, thus identifying the optimal among them. Lastly, as a complement to the fabrication study, the filtration permeability of the optimal membrane was evaluated using deionized water. This work thus paves the way towards the fabrication of ceramic membranes based on B_4C, lighter and potentially more durable than others, for filtration applications.

1. Introduction

Sustainable consumption of water, an essential, irreplaceable, and increasingly scarce resource, is today a global concern that requires particular attention for policies of action worldwide [1]. An integral part of such policies is the purification of wastewaters and secondary effluents as a substitute for freshwater for certain uses, including recycling potable water [1]. This explains the widespread growing interest in all technologies of wastewater reclamation in general, and in the still recent membrane filtration technologies in particular [2–4]. These latter have the same efficiency as other more conventional technologies (*e.g.*, coagulation, flocculation, ion exchange, *etc.* [5–7]), and are very environmentally friendly (because chemicals are used only for membrane cleaning), cost-effective (because the capital investment and the costs of both use and maintenance are lower), and practical (because the filtration stations are easier to operate, much more compact, easily scalable, and very versatile) [8–10].

The development of ceramic membranes is still in a relatively incipient stage and, while they do not yet dominate the market, it is already widely recognised that they are preferable over polymeric membranes in terms of both performance (*i.e.*, greater permeability and selectivity), operability, and durability (*i.e.*, superior mechanical robustness and lesser susceptibility to fouling) [10–14]. SiC membranes stand out among the current ceramic membranes [10,11]. Comparatively, SiC has greater hardness, abrasion resistance, refractoriness, and chemical inertness than the typical oxides (*e.g.*, Al_2O_3, SiO_2, and TiO_2) which most ceramic membranes are made of, and therefore those of SiC are intrinsically more durable and suitable for harsher filtration conditions. Moreover, they also have superior hydrothermal stability, higher water permeability, and greater fouling resistance, a highly desirable combination of properties in any filtration membrane. Unsurprisingly, SiC membranes are currently already a commercial product on the market for the purification of liquids and gases [11]. Very interestingly, membranes made with other advanced carbides could also be appealing, and thus worthy of study and development. This could be the case for B_4C, which in principle offers at least two important advantages over SiC. First, it is harder (*i.e.*, 35 GPa or more *vs* 25 GPa or less) and thus less abradable, so it would yield more durable membranes. And second, it is less dense (*i.e.*, ~2.52 g/cm^3 *vs* ~3.21 g/cm^3), and therefore it would yield lighter membranes. These two expectations are derived for B_4C and

* Corresponding author.
E-mail address: alortiz@unex.es (A.L. Ortiz).

https://doi.org/10.1016/j.jeurceramsoc.2022.02.035
Received 8 October 2021; Received in revised form 3 February 2022; Accepted 13 February 2022
Available online 17 February 2022

SiC membranes having the same thickness and degree of densification. Consequently, the same properties that make sintered (dense) B_4C the material of choice for ceramic armours and water-jet cutting tools, to name just two uses, could also make partially sintered (porous) B_4C very attractive as filtration ceramic membranes. Also, B_4C is hardly densifiable at all by solid-state sintering, which is nothing but a plus for the fabrication of ceramic membranes (by definition, porous materials).

With these premises in mind, this study was aimed at fabricating and characterising, for the first time, B_4C ultrafiltration membranes. Given that there is no earlier work on the preparation of B_4C membranes, this first study focuses mainly on aspects of ceramic processing/sintering, describing the complete fabrication sequence and microstructural-textural-mechanical characterisation of these membranes. Nonetheless, a preliminary test of permeability to deionized water (*i.e.*, flux measurement) will also be presented as a first evaluation of their filtration performance.

2. Experimental procedure

The present B_4C membranes were fabricated from a custom-made colloidal ceramic slurry, which was deposited by dip-coating onto proprietary SiC supports and then pressureless sintered. Briefly, a commercially available powder of B_4C (d_{50} ~0.6–0.9 μm; Grade HD 15, Hönagäs AB, Sweden) was acquired, and used as-received. A semi-dilute B_4C slurry (*i.e.*, with only ~8 vol% B_4C) was prepared by aqueous colloidal processing at neutral pH, by dispersing appropriately the B_4C powder in de-ionized water to a solid loading of 18 wt%, using 2 wt% of diluted (1:10) polyethylenimine (PEI; MW ~25000; Sigma-Aldrich, USA) as deflocculant, and 1 wt% of polysaccharide dicarbonic acid polymer (Optapix CS-76; Zschimmer & Schwarz, Germany) as binder, and sonicating at 100 W (UP400S, Hielscher, Germany) until complete dispersion. The optimal sonication time was identified by measurements of the particle size distribution by laser diffraction (LD; S3500, Microtrack MRB, USA). Finally, the optimally-sonicated B_4C slurry was characterized rheologically to measure its viscosity curve, using a rheometer (MCR 302e, Anton Paar, Austria) configured in the cone (0.5°)-plate geometry and operated in controlled shear rate mode. As reference for comparison, the viscosity curve of the de-ionized water used to prepare the B_4C slurry was also measured.

Next, green membranes were prepared by depositing the B_4C slurry onto SiC supports supplied by LiqTech Ceramics A/S, and then drying. In particular, multi-channeled highly-porous rectangular flat substrates were used, designed for submerged outside-in vacuum-driven filtration. These are the same as the company uses for one of its commercial SiC membranes and for one of its currently under development hybrid SiC+ZrO_2 membranes [15]. According to the manufacturer's specifications and earlier studies [10,15], these SiC supports have a strength of ~30 MPa, total porosity of ~40%, average pore size of ~15 μm, and water permeability of ~12000 l/(m^2·h·bar). The B_4C slurry was deposited by dip-coating using a custom-made device operated at a withdrawal rate of ~17 mm/s, with dipping times of 20 s and 30 s.[1] The membranes were then allowed to dry at ambient conditions overnight, and the entire coating process was repeated once more. The resulting green membranes were examined by scanning electron microscopy (SEM; 3600 N, Hitachi, Japan) in both plane and cross-sectional views to evaluate their surface quality and thickness, respectively.

The green membranes were subsequently pressureless sintered in a graphite furnace (resistance graphite furnace, Graphite Furnace Systems, USA) at two different temperatures for 1.5 h under a flowing high-purity Ar atmosphere. The exact sintering cycle is confidential information of LiqTech Ceramics A/S, and is therefore unavailable. Therefore, one of the sintering temperatures will be denoted simply as T, and the other as T+65 °C, with both T and T+65 °C lying in the range 1800–1950 °C. Once sintered, the membranes were calcined (ELS 1000 S SOB, Helmut Rohde GmbH, Germany) in air at 450 °C for 30 min (using 200 °C/h heating and cooling ramps) to remove any possible free carbon blocking the smallest pores. These calcination conditions were selected on the basis of a combined study of thermogravimetry (TG; STA 449 F3 Jupiter, Netzsch, Germany) coupled with mass spectrometry (MS; QMS 403D AëolosIII, Netzsch, Germany) performed on powders extracted from one of the sintered membranes by scratching. The TG-MS study was carried out under flowing simulated air (*i.e.*, 50 ml/min of 20%O_2+80%Ar) because, if it had been done in air (whose composition is ~20%O_2+80%N_2), it would not have been possible to monitor the emission of CO gas (since N_2 and CO have the same mass of 28 u).

Lastly, the sintered+calcined membranes were characterised in detail. First, they were all characterised microstructurally by SEM, so as to select those appropriate for further study. Second, those selected were characterised texturally by capillary flow porometry (CFP; Quantachrome 3G zh, Anton Paar, Austria) using Porofil™ as wetting fluid to measure their open interconnected pore size distribution, and also mechanically by scratch tests (Revetest RST3, Anton Paar, Graz, Austria) at 1 N load to compare qualitatively their abrasion resistance. This enabled the optimal membrane to be identified. And finally, as a complement to the fabrication study, a first preliminary evaluation of the filtration performance of the optimal membrane was also conducted. Specifically, its permeability to deionised water was evaluated by measuring the flux as a function of the transmembrane pressure.

3. Results and discussion

3.1. Slurry and green membranes

Fig. 1 shows the particle size distribution of the B_4C slurry for different sonication times, as determined by LD. It can be seen that the unsonicated slurry exhibits a bi-modal particle size distribution, mostly containing fine particles with sizes in the range ~0.2–1.5 μm together with some coarse and super-coarse agglomerates whose sizes vary widely in the range ~7–110 μm. This is undesirable because it will result in heterogeneous membranes. These agglomerates did not form during aqueous colloidal processing, but were present in the as-received powders because, at neutral pH, B_4C deflocculated with PEI has a large zeta potential that ensures the repulsiveness of the particles in water [16–18]. However, the agglomerates are soft because they broke up with the "smooth" 100 W sonication. Indeed, it can be seen that only 10 Ws/ml sonication was already sufficient to obtain a slurry with a mono-modal distribution of fine particles, from which homogenous membranes can be obtained. Increasing the sonication from 10 Ws/ml to 50 Ws/ml did not affect the particle sizes, because the "smooth" sonication at 100 W does not break the single B_4C particles into smaller fragments, but, although not needed, it is definitively recommendable to ensure a proper dispersion of the B_4C particles in the water. Also, neither the subsequent binder addition nor the subsequent sonication for another 10 Ws/ml to disperse it had any detrimental effect on the dispersion. Therefore, 50 Ws/ml sonication + binder addition + 10 Ws/ml sonication were the dispersion conditions used to prepare the B_4C slurry for dip-coating.

By way of example, Fig. 2 shows optical photographs of some green pieces (*i.e.*, B_4C membrane on SiC support) fabricated. It can be seen that the membranes covered the supports uniformly, indicating that the adequate formulation of the B_4C slurry provided it with the desired pourable consistency and wettability on the SiC supports. In turn, the substrates drained the water of the slurry also adequately, making "slip casting" feasible. Indeed, earlier studies have shown that B_4C slurries of this type or similar are fully suitable for slip casting operations because they are well-deflocculated and have shear-thinning rheological behaviours with low viscosity and thixotropy [16,19,20]. Certainly, Fig. 3

[1] Prior to dip-coating, the lateral contours of the SiC supports were sealed with liquid latex to prevent the B_4C slurry from penetrating the interior and the channels.

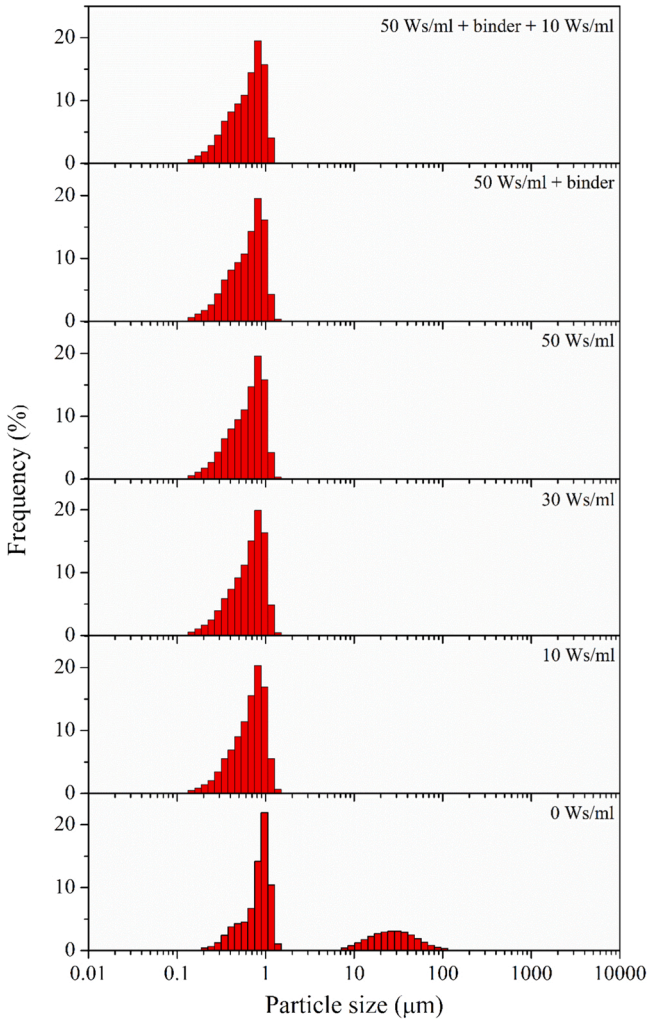

Fig. 1. Particle size distribution in the B_4C slurry for different sonication conditions, as determined by LD.

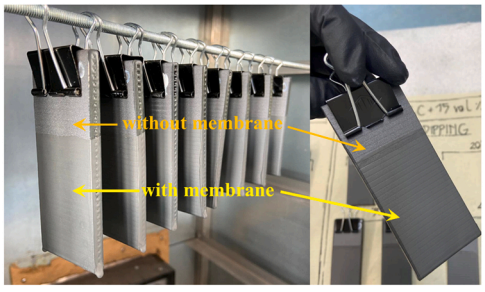

Fig. 2. Optical photographs of the green pieces (*i.e.*, B_4C membranes deposited onto the SiC supports).

shows the viscosity curve of the B_4C slurry demonstrating that it is indeed slightly shear-thinning and extremely fluid (for example, its viscosity at 100 s^{-1} is as low as ~0.002 Pa·s), and only slightly more viscous than the de-ionized water used as dispersion medium. This is due to the low contents of B_4C (~8 vol%), deflocculant (2 wt%), and binder (1 wt%) used in its formulation. Also importantly, the green pieces were found to be robust, possessing the sufficient strength as to have good manageability, storability, dry trimmability, *etc*.

Fig. 4 shows SEM images representative of the top surface of the green membranes dip-coated for 20 s and 30 s. It can be seen in the low-magnification micrographs (left panel) that they are essentially free of macro-cracks or other macro-defects (*i.e.*, voids, bubbles, pin holes, *etc.*), and that they are very homogeneous. It can also be seen in the higher-magnification micrographs (right panel) that they have the expected porous microstructure, with good particle packing and without micro-cracks or other micro-defects.

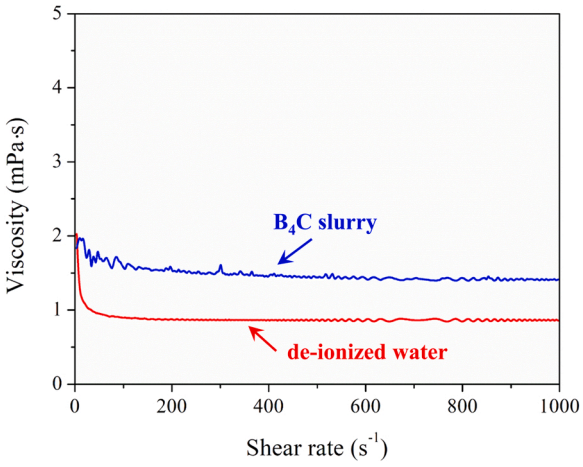

Fig. 3. Dependence of the viscosity on the shear rate for the B_4C slurry.

Fig. 5 shows SEM images representative of the cross-sectional fracture surface of the green membranes dip-coated for 20 s and 30 s. It can be seen in Fig. 5A-B that they are also free of through-thickness macro- and micro-defects, and that there is good adhesion between the B_4C membrane and the SiC support as evidenced by the absence of delamination, spalling, or interfacial fracture. This became more evident in making the extensive higher-magnification SEM observations, an example of which is shown in Fig. 5C. It is also evident in Fig. 5C that there is a vast difference in the microstructural scales of the B_4C membrane (fine-particulate; ~0.6–0.9 μm average particle size) and SiC support (super-coarse-particulate; ~35–38 μm average particle size). The mean thickness of the green membranes determined from the numerous SEM observations is included in Fig. 5A-B. It can be seen that they have green thicknesses of the order of two or three tens of microns, which is not bad because, as seen in Fig. 5D, below the membrane a transition zone was formed within the support that is also useful for filtration, with fine B_4C particles located in the interstitials between the large SiC particles. The green membranes are not thicker due to the use of a semi-dilute B_4C slurry and only two dipping repetitions. Also, the formation of the transition zone is because, with its extremely low viscosity, the B_4C slurry infiltrated the SiC supports to a certain depth. Indeed, as observed in Fig. 5E, the depth of infiltrated zone is much greater than the membrane thickness, and not less than 100 μm. Comparatively, it is also clear that increasing the dip-coating time from 20 s to 30 s resulted in slightly thicker green membranes, which is simply because in drain casting the cast grows proportionally to the square root of the casting time (*i.e.*, capillary suction of water into the SiC support concentrates and coagulates the B_4C particles in the slurry at the support surface, forming and growing the cast). Certainly, for uniaxial filtration, as is the present case, the cast thickness D as a function of casting time t is given by the approximate equation [21]:

$$D \simeq \left(\frac{2J\Delta P K_P}{\mu} t\right)^{0.5}$$

where J is the volume of cast/volume of liquid removed, ΔP the apparent mold suction, K_P the liquid permeability of the cast, and μ the viscosity of the liquid transported.

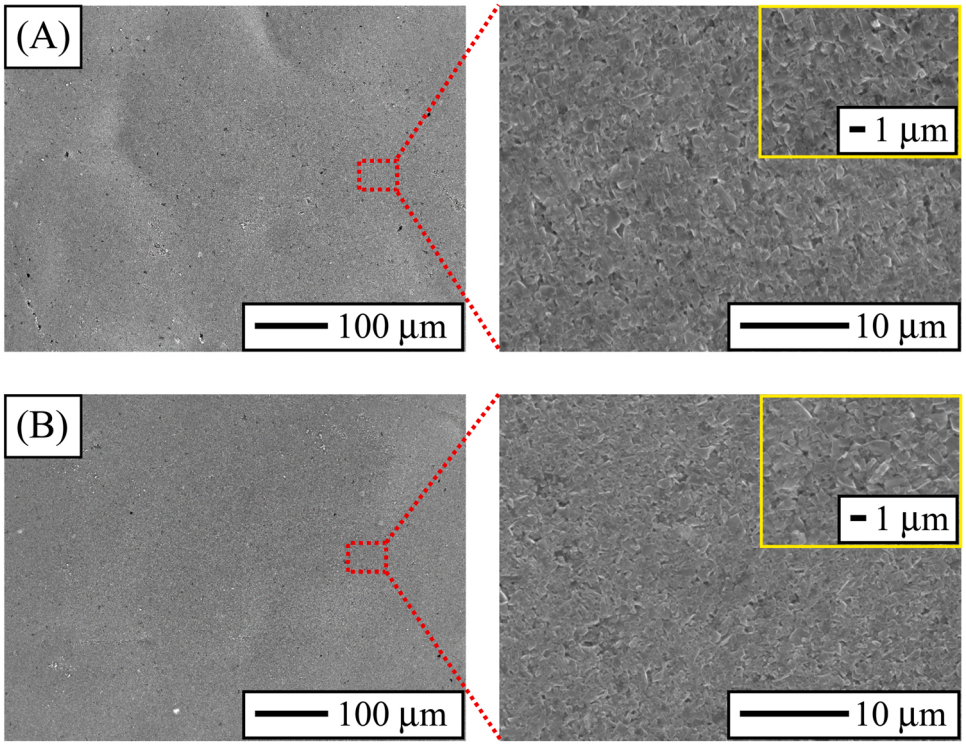

Fig. 4. SEM micrographs representative of the top surface of the green membranes obtained by dip-coating the B_4C slurry for (A) 20 s and (B) 30 s. The left panel shows low-magnification micrographs giving a general view, and the right panel (and the inserts therein) higher-magnification micrographs showing more details. These SEM images were all taken using secondary electrons.

3.2. Sintered membranes

The two sets of green membranes prepared were pressureless sintered at temperature T or T+65 °C for 1.5 h (as mentioned above, both in the range of 1800–1950 °C), after which they were calcined in air to clean them from possible free carbon (impurities from the starting powders, or picked up during sintering in the graphite furnace) blocking the smaller pores. Figs. 6 and 7 show the results of two TG-MS tests performed on powders extracted from one of the sintered membranes to elucidate the optimal calcination conditions (*i.e.*, temperature and time). In a first TG-MS test, the mass variation of the membrane and the emission of CO_2 and CO gases were registered as functions of calcination temperature up to 1000 °C, the results of which are shown in Fig. 6. Three temperature intervals are distinguishable. Up ~450 °C there is increasing mass loss together with increasing emission of both CO_2 and CO. Between ~450 °C and ~650 °C there is neither mass loss or mass gain, the emission of CO drops abruptly, and that of CO_2, also falling, is still intense and with a second release peak at ~475 °C. Lastly, from ~650 °C onwards there is increasing mass gain together with decreasing emission of both CO_2 and CO. The possible reactions occurring during the calcination of the membrane in air are [22]:

$$C+O_2(g)\rightarrow CO_2(g) \quad (1)$$

$$C+1/2O_2(g)\rightarrow CO(g) \quad (2)$$

$$B_4C+4O_2\rightarrow 2B_2O_3+CO_2(g) \quad (3)$$

$$B_4C+7/2O_2\rightarrow 2B_2O_3+CO(g) \quad (4)$$

Reactions (1) and (2) consume carbon by forming CO_2 or CO gas, respectively, therefore causing mass loss. Reactions (3) and (4) oxidize B_4C forming B_2O_3, therefore causing mass gain (~152% for the complete oxidation). Consequently, taken together, the TG and the gas emission curves suggest (*i*) that up to ~450 °C some free carbon in the membrane is progressively eliminated without oxidizing the latter, (*ii*) that in the temperature range ~450–650 °C, part of the still remaining residual free carbon in the membrane is eliminated while the latter begins to oxidize, and (*iii*) that from ~650 °C onwards the B_4C membrane becomes more oxidized but little because the mass gain is only ~0.5%. Therefore, ~450 °C seemed to be the optimal calcination temperature.

With the above information, in a second TG-MS test the mass variation of the membrane and the emission of both CO_2 and CO gases were registered at 450 °C as functions of calcination time up to 1 h, the results of which are shown in Fig. 7. It can be seen that some free carbon in the membrane is eliminated during the heating ramp up to 450 °C, and that above ~5 min the exposure time at 450 °C does not seem to play a role. Nonetheless, the calcination time at 450 °C was set at 30 min to ensure that large membranes prepared at industrial scale would reach thermal equilibrium.[2] In any case, it is likely that the calcination at 450 °C is too smooth to completely remove the free carbon from the membrane.

Fig. 8 shows SEM images representative of the top surface of all membranes once sintered and calcined. It can be seen that while those sintered at temperature T are free of micro/meso-cracks (Fig. 8A-B), those sintered at temperature T+65 °C are clearly cracked (Fig. 8C-D). The latter are therefore unsuitable, and were excluded from further study. These cracks most likely formed during the last cooling segment of the sintering cycle because the greater densification of the membranes sintered at temperature T+65 °C reduced their strain tolerance. On the contrary, the greater porosity of the membranes sintered at temperature T did enable them to successfully tolerate the lower thermal residual stresses inherent to the co-sintering of B_4C (membrane) and SiC (support). Note that, because B_4C has a greater thermal expansion coefficient

[2] For example, LiqTech Ceramics A/S fabricates flat sheet membranes and tubular membranes with dimensions as large as ~100 mm (width) × 500 mm (length) × 6 mm (thickness) and ~25 mm (diameter) × 1178 mm (length), respectively.

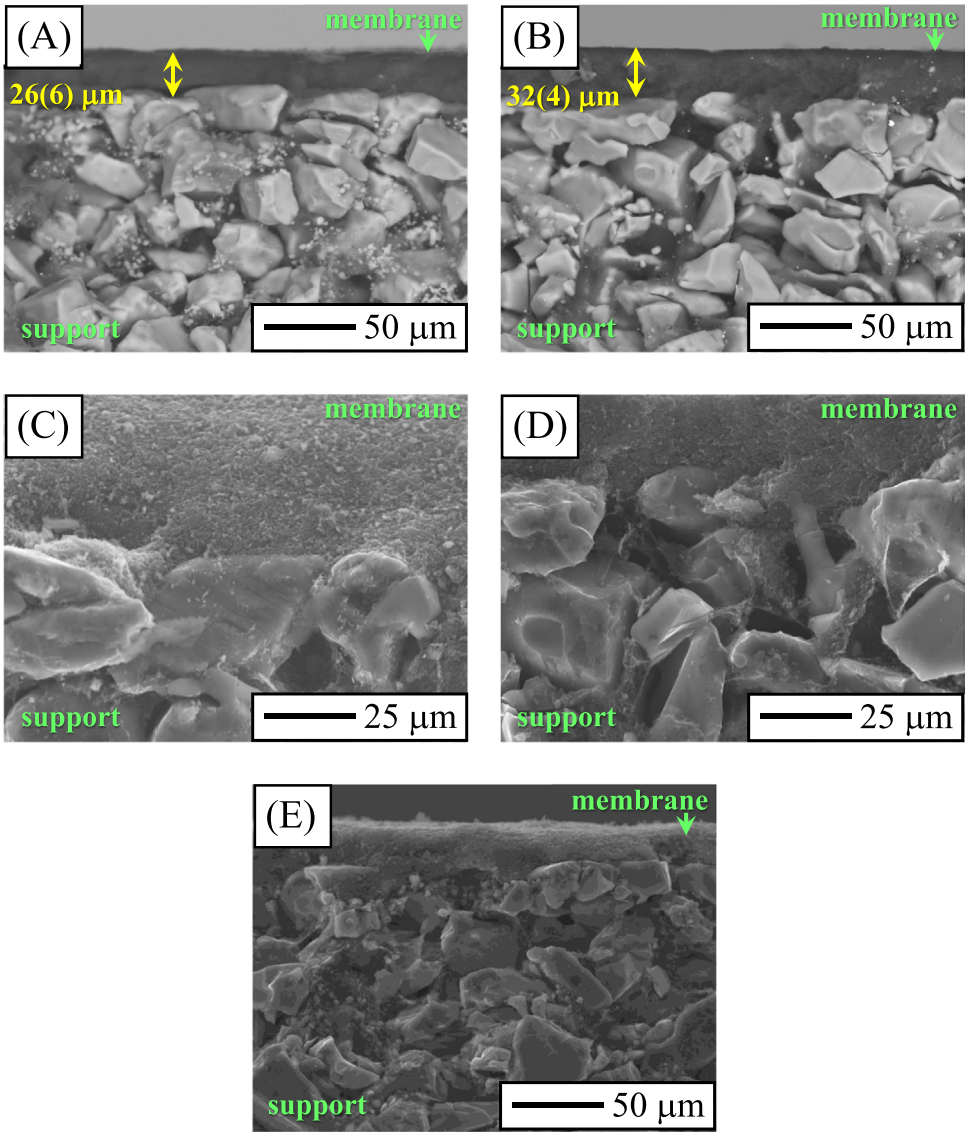

Fig. 5. SEM micrographs representative of the cross-sectional fracture surface of the green membranes obtained by dip-coating the B_4C slurry for (A) 20 s, (B)-(C)-(D) 30 s, and (D) 20 s. The SEM images in (A) and (B) were taken using backscattered electrons, and those in (C)-(D)-(E) using secondary electrons. The numbers in (A) and (B) are the corresponding mean membrane thicknesses.

than SiC (*i.e.*, $\sim 6.53 \cdot 10^{-6}\ ^{\circ}C^{-1}$ *vs* $\sim 4.5 \cdot 10^{-6}\ ^{\circ}C^{-1}$), an in-plane tensile stress arises in the membrane during the cooling segment. Also note that the magnitude of such a tensile stress increases with increasing sintering temperature [23], which facilitates the appearance and propagation of cracks in the membrane. Specifically, the residual stress (σ_R) obeys the relationship $\sigma_R \propto \Delta\alpha \cdot \Delta T$, where $\Delta\alpha$ is the thermal expansion mismatch between the support and membrane and ΔT is the temperature difference between the sintering temperature and room temperature. Fig. 9 shows SEM images of the two membranes sintered at temperature T+65 °C prior to their calcination at 450 °C for 30 min demonstrating that, as expected, cracking occurs during sintering, not during the subsequent calcination. Indeed, calcination, if any at all, could help to self-heal some defects.

Fig. 10 shows SEM images representative of the cross-sectional fracture surface of the crack-free membranes. Essentially, they are as thick as their corresponding green membranes (*i.e.*, thicknesses in the order of two or three tens of microns), indicating that sintering at temperature T caused at most negligible and possibly no shrinkage by densification. This, which is indeed desirable to obtain porous membranes, is because T was intentionally chosen sufficiently low (*i.e.*, T+65 °C in the range 1800–1950 °C) for B_4C to be "undensifiable" by conventional pressureless sintering. Indeed, the higher-magnification SEM images in Fig. 11 representative of the top surface of these crack-free membranes confirm that they reached only the intermediate sintering regime. This is the desirable scenario because the membranes thus retain an open interconnected pore structure and a degree of porosity that ensures their permeability, while they also develop an interparticle neck that ensures their sufficient mechanical integrity [24]. "Under-densification" within the initial sintering regime is undesirable because the interparticle neck would be minimal [24], and therefore the membranes would lack mechanical integrity. "Over-densification" within the final sintering regime is also undesirable because the porosity would be much lower and the pore structure would collapse into closed isolated porosity [24], and therefore the membranes would not be permeable.

3.3. Selection and performance of the optimal membrane

Fig. 12 shows the interconnected pore size distributions measured by CFP of the crack-free membranes sintered at temperature T and then calcined, and Fig. 13 the scratches made on them. It can be seen in

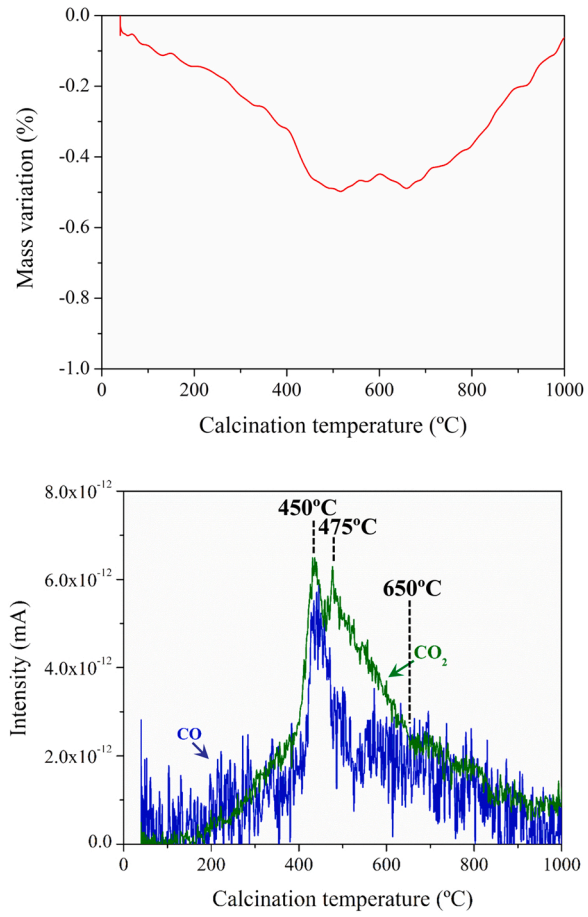

Fig. 6. Curves of TG and gas emission (*i.e.*, release of CO and CO_2) of the membranes, registered as functions of the calcination temperature (in the range 40–1000 °C). The test was performed under flowing simulated air (*i.e.*, 20% O_2+80%Ar) on the powder extracted from one of the membranes sintered at temperature *T*.

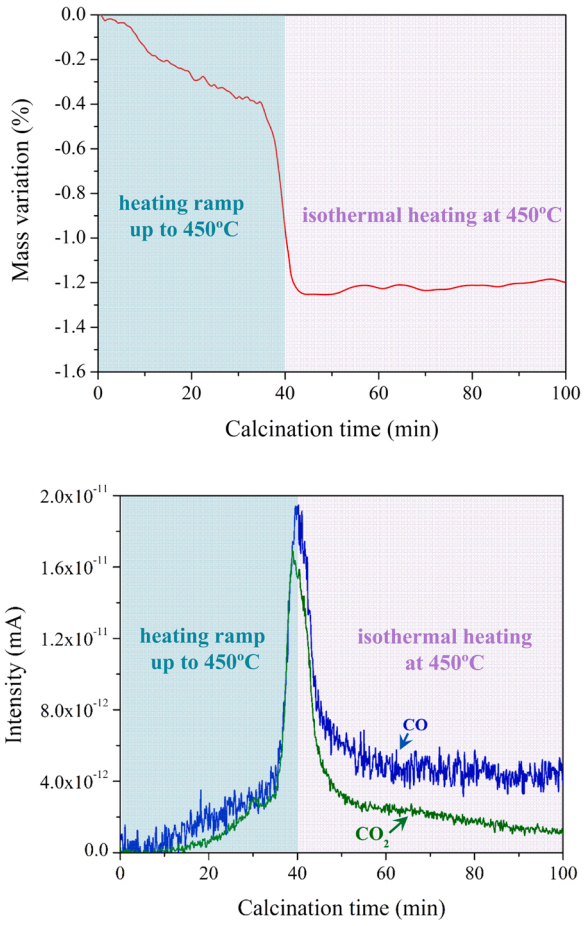

Fig. 7. Curves of TG and gas emission (*i.e.*, release of CO and CO_2) of the membranes, registered as functions of the calcination time for up to 1 h at 450 °C. The test was performed under flowing simulated air (*i.e.*, 20%O_2+80% Ar) on the powder extracted from one of the membranes sintered at temperature *T*.

Fig. 12 that the membrane prepared for a dip-coating time of 20 s exhibits a poorly-defined and relatively broad pore size distribution, without a uniform apparent pore size. The membrane prepared for a dip-coating time of 30 s, however, displays a well-defined, sharp, and narrow pore size distribution, with pore sizes only in the range ~67–110 nm (mode ~72 nm). This last porosity is much more desirable in terms of ultrafiltration. Moreover, Fig. 13 shows that the former has lower scratch resistance than the latter (*i.e.*, the scratch width is ~20% greater and there is notable particle pull-out), indicative of it being less robust mechanically and of poorer durability under abrasive feeds. Therefore, the membrane prepared for a dip-coating time of 30 s is preferable in terms of both filtration permeability and durability. This is so because, as inferred from the SEM images in Fig. 11, it must have reached a slightly greater densification during sintering, developing a smaller pore size and better particle cohesion. The sintering conditions were the same in both cases, and therefore its greater densification in turn would be the result of its greater green densification, something that the SEM observations on the green membranes appear to support (Fig. 4).

Finally, to complement the fabrication study, Fig. 14 shows the results of the preliminary filtration test using deionized water of the optimal membrane. It can be seen that the permeate flux increases linearly with increasing transmembrane pressure, as expected for non-fouling filtration. Therefore, the membrane permeability could be calculated by a linear fit to the experimental data, and was found to be ~80(4) l/(m^2·h·bar). There are no earlier filtration data for B_4C membranes to compare with because this is the first time they have been fabricated. Nonetheless, this permeability is a little low relative to other membranes deposited onto similar SiC supports. Thus for example, SiC membranes with thickness in the range 20–45 μm and pore sizes within the range 0.2–1.4 μm have permeabilities in the order of 4000 l/(m^2·h·bar) [10], and ZrO_2 membranes with ~45 μm thickness and pore sizes in the range 50–70 nm have it of ~360 l/(m^2·h·bar) [15]. While the B_4C and ZrO_2 membranes have relatively comparable permeabilities because they are both ultrafiltration membranes, those of SiC have much higher permeability because they are microfiltration membranes. Given that the B_4C membrane is not especially thick, its relatively low permeability could be due (*i*) to the small (nanoscale) mode pore size, and (*ii*) to the intermediate layer of B_4C infiltrated into the SiC support, both of which would reduce the permeate flux, and most likely also (*iii*) to the less-hydrophilic nature of the membrane itself reducing the affinity to water. Causes (*i*) and (*ii*) are microstructural, and are therefore, if desired, in principle solvable by judiciously ceramic processing/sintering. Cause (*iii*), if confirmed in future work, could be intrinsic to B_4C, or attributable to the presence of some hydrophobic free carbon. The former could also be, in principle, solvable by post-sintering chemical functionalization of the membranes, and the former by using more demanding calcination conditions. In any case, none of this should be interpreted negatively because today there is a growing interest in the development of both (*i*) ceramic ultrafiltration membranes, which are inherently less permeable than their microfiltration counterparts, and (*ii*) hydrophobic ceramic membranes to thus extend the range of

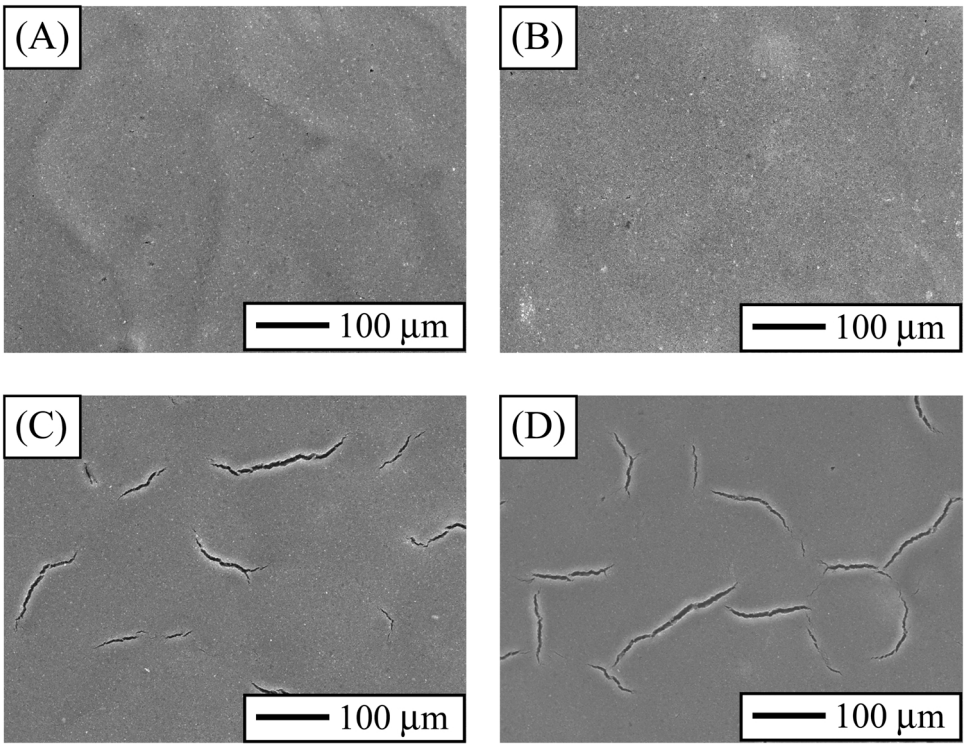

Fig. 8. SEM micrographs representative of the top surface of the sintered+calcined membranes obtained from the B_4C slurry under the following dip-coating time and sintering temperature conditions: (A) 20 s and *T*, (B) 30 s and *T*, (C) 20 s and *T*+65 °C, and (D) 30 s and *T*+65 °C. These SEM images were all taken using secondary electrons.

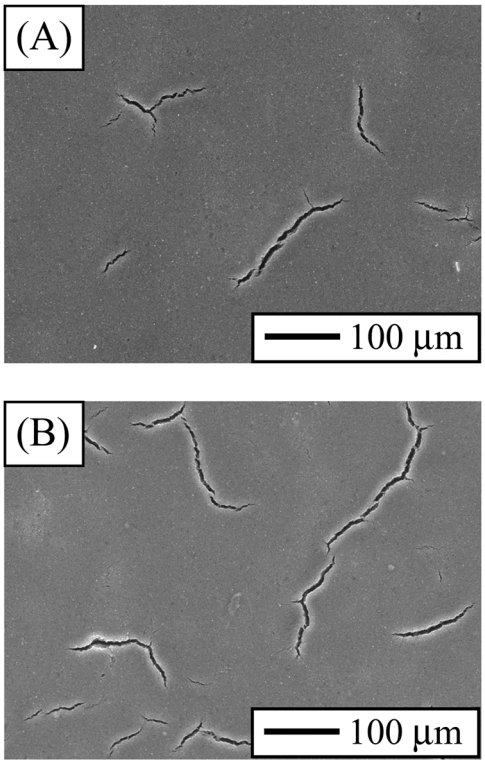

Fig. 9. SEM micrographs representative of the top surface of the sintered membranes obtained from the B_4C slurry under the following dip-coating time and sintering temperature conditions: (A) 20 s and *T*+65 °C, and (D) 30 s and *T*+65 °C. Both SEM images were taken using secondary electrons.

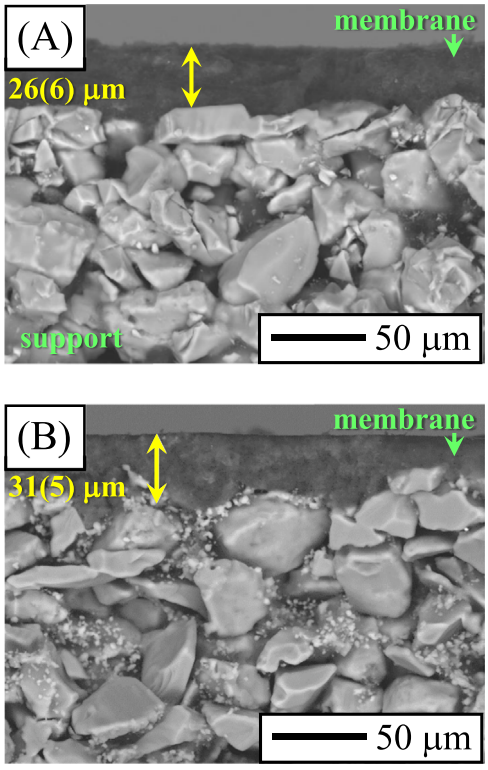

Fig. 10. SEM micrographs representative of the cross-sectional fracture surface of the crack-free membranes obtained by dip-coating the B_4C slurry for (A) 20 s and (B) 30 s, and then sintering at temperature *T* and calcining at 450 °C for 30 min. Both SEM images were taken using backscattered electrons. The numbers are the corresponding mean membrane thicknesses.

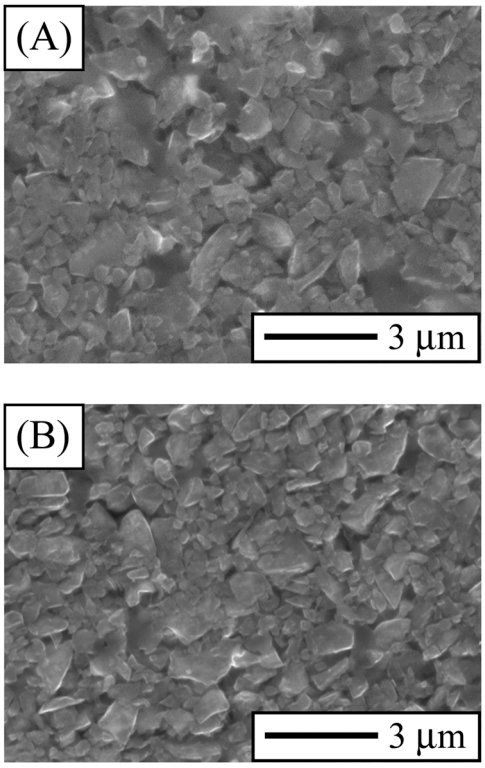

Fig. 11. SEM micrographs representative of the top surface of the crack-free membranes obtained by dip-coating the B_4C slurry for (A) 20 s and (B) 30 s, and then sintering at temperature *T* and calcining at 450 °C for 30 min. Both SEM images were taken using secondary electrons.

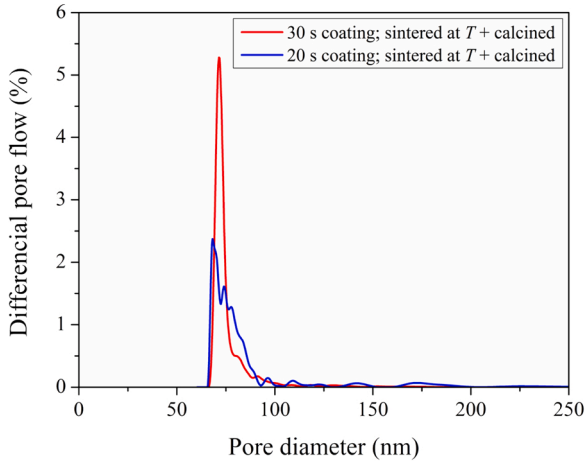

Fig. 12. Distributions of interconnected open pore sizes, as determined by CFP, for the crack-free membranes obtained by dip-coating the B_4C slurry for 20 s and 30 s, and then sintering at temperature *T* and calcining at 450 °C for 30 min.

application of their hydrophilic counterparts.

3.4. Final remarks

To conclude, it is worth re-emphasizing some final considerations. What is remarkable is that the B_4C membranes deserve further study and development. First, the superior hardness of B_4C is expected to be a plus in terms of durability, an important attribute always but much more in applications involving the filtration of abrasive feeds. And secondly, B_4C is exceptionally lightweight, another important attribute to reduce

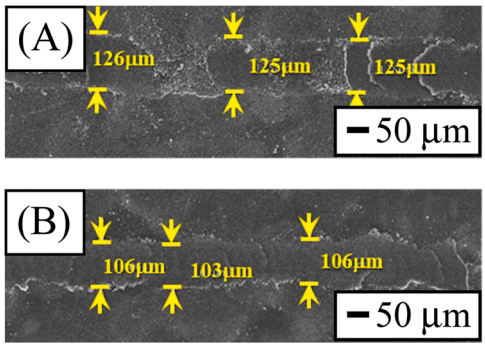

Fig. 13. SEM micrographs representative of the scratching performed on the crack-free membranes obtained by dip-coating the B_4C slurry for (A) 20 s and (B) 30 s, and then sintering at temperature *T* and calcining at 450 °C for 30 min. The numbers indicate the width of the scratches measured at various locations.

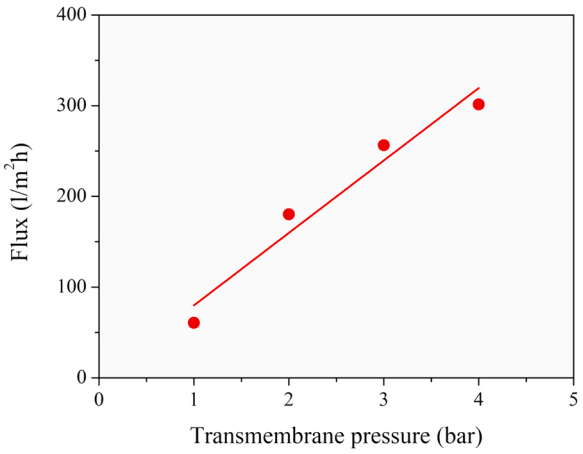

Fig. 14. Curve of filtration permeability (*i.e.*, permeate flux *vs* transmembrane pressure) of the crack-free membrane obtained by dip-coating the B_4C slurry for 30 s, and then sintering at temperature *T* and calcining at 450 °C for 30 min. The dots are the experimental data, and the solid line a linear fit to them.

spurious weight in large filtration units, especially if in the future the B_4C membranes are also deposited onto B_4C supports (yet undeveloped). Future processing/sintering efforts are therefore expected aimed at further optimizing the features of the B_4C membranes. Thus for example, in principle their thickness could be adjustable on demand by tailoring the formulation of the slurry, the dipping time, and the multiplicity of the dip-coating (specifically, the greater the loads of B_4C and binder, the immersion time, and the number of repetitions, the greater the thickness). Their porosity and pore size distribution could be potentially adjustable to a certain extent by the appropriate choice of the starting B_4C powders (because the smaller the particles, the smaller the interstitial voids) and by tailoring the sintering cycle (specifically, the lower the temperature and shorter the time, the greater the porosity and the larger the pore size). All this, together with compositional effects (*i.e.*, residual graphite and B_2O_3/H_3BO_3 impurities), dictate the filtration performance (in particular, the permeability and fouling). Their hydrophilicity/hydrophobicity and antifouling also depend on their composition, and, if needed/desired, can also be in principle modulable by compositional adjustment and/or by tailoring their surface chemistry *via* surface engineering (*i.e.*, modification and/or functionalization). Lastly, it is acknowledged that it also remains for the future to perform fundamental mechanical–microstructural studies as well as detailed filtration studies on the B_4C membranes, these last both under model conditions and conditions that are nominally representative of actual practical applications. However, all this is beyond the scope of this first

processing/sintering study.

4. Conclusions

A study was conducted of the fabrication of B_4C membranes, deposited onto SiC porous substrates, for ultrafiltration applications. Based on the experimental results and analyses, the following conclusions can be drawn:

1. A semi-dilute B_4C slurry can be prepared in an environmentally-friendly manner by aqueous colloidal processing that allows robust green membranes on porous substrates to be obtained by dip-coating.
2. Pressureless sintering, if done appropriately, bonds the B_4C particles together, developing an interparticle neck while causing negligible densification and therefore shrinkage of the membrane. Crack-free membranes can thus be obtained having both an interconnected open porosity and the required mechanical integrity.
3. Calcination in air under smooth conditions of temperature and time is usefully applicable to cleanse the membranes from possible free carbon, with hardly any B_4C oxidation.
4. The present B_4C membranes are potentially suitable for ultrafiltration applications. Future study is nonetheless still needed aimed at further optimizing these membranes by judicious ceramic processing/sintering.

Declaration of Competing Interest

The authors declare that they have no known competing financial interests or personal relationships that could have appeared to influence the work reported in this paper.

Acknowledgements

Cristina Ojalvo thanks the JECS Trust for her mobility Grant no. 2020238, and the Junta de Extremadura for her PhD Grant no. PD16027. This work was also supported by the Junta de Extremadura under Grants no. IB20017 and GR18149 (co-financed with FEDER funds).

References

[1] SDG 6 Synthesis Report, 2018 on Water and Sanitation, United Nations. ⟨https://www.unwater.org/app/uploads/2018/12/SDG6_SynthesisReport2018_WaterandSanitation_04122018.pdf⟩.
[2] C. Reith, B. Birkenhead, Membranes enabling the affordable and cost effective reuse of wastewater as an alternative water source, Desalination 117 (1–3) (1998) 203–209.
[3] J.L. Acero, F.J. Benitez, A.I. Leal, F.J. Real, F. Teva, Membrane filtration technologies applied to municipal secondary effluents for potential reuse, J. Hazard. Mater. 177 (1–3) (2010) 390–398.
[4] A. Farsi, S.H. Jensen, P. Roslev, V. Boffa, M.L. Christensen, Inorganic membranes for the recovery of effluent from municipal wastewater treatment plants, Ind. Eng. Chem. Res. 54 (13) (2015) 3462–3472.
[5] M. Kang, H. Chen, Y. Sato, T. Kamei, Y. Magara, Rapid and economical indicator for evaluating arsenic removal with minimum aluminum residual during coagulation process, Water Res. 37 (19) (2003) 4599–4604.
[6] J. Zhong, X. Sun, C. Wang, Treatment of oily wastewater produced from refinery processes using flocculation and ceramic membrane filtration, Sep. Purif. Technol. 32 (1–3) (2003) 93–98.
[7] A. Alshameri, A. Ibrahim, A.M. Assabri, X. Lei, H. Wang, C. Yan, The investigation into the ammonium removal performance of Yemeni natural zeolite: modification, ion exchange mechanism, and thermodynamics, Powder Technol. 258 (2014) 20–31.
[8] P.S. Goh, A.F. Ismail, A review on inorganic membranes for desalination and wastewater treatment, Desalination 434 (2018) 60–80.
[9] M. Kamali, D.P. Suhas, M.E. Costa, I. Capela, T.M. Aminabhavi, Sustainability considerations in membrane-based technologies for industrial effluents treatment, Chem. Eng. J. 368 (2019) 474–494.
[10] E. Eray, V. Boffa, M.K. Jørgensen, G. Magnacca, V.M. Candelario, Enhanced fabrication of silicon carbide membranes for wastewater treatment: from laboratory to industrial scale, J. Membr. Sci. 606 (2020), 118080.
[11] E. Eray, V.M. Candelario, V. Boffa, H. Safafar, D.N. Østedgaard-Munck, N. Zahrtmann, H. Kadrispahic, M.K. Jørgensen, A roadmap for the development and applications of silicon carbide membranes for liquid filtration: recent advancements, challenges, and perspectives, Chem. Eng. J. 414 (2021), 128826.
[12] B. Hofs, J. Ogier, D. Vries, E.F. Beerendonk, E.R. Cornelisssen, Comparison of ceramic and polymeric membrane permeability and fouling using surface water, Sep. Purif. Technol. 79 (3) (2011) 365–374.
[13] Z. He, Z. Lyu, Q. Gu, L. Zhang, J. Wang, Ceramic-based membranes for water and wastewater treatment, Colloids Surf. A 578 (2019), 123513.
[14] S. Geno Lehman, L. Liu, Application of ceramic membranes with pre-ozonation for treatment of secondary wastewater effluent, Water Res. 43 (7) (2009) 2020–2028.
[15] F.E. Bortot, N.N. Coelho, G. Kaiser, V.M. Magnacca, Candelario, Corrosion resistant ZrO2/SiC ultrafiltration membranes for wastewater treatment and operation in harsh environments, J. Eur. Ceram. Soc. 41 (15) (2021) 7792–7806.
[16] C. Ojalvo, R. Moreno, F. Guiberteau, A.L. Ortiz, Manufacturing B_4C parts with Ti-Al intermetallics by aqueous colloidal processing, J. Eur. Ceram. Soc. 40 (2) (2020) 226–233.
[17] C. Ojalvo, V. Zamora, R. Moreno, F. Guiberteau, O. Borrero-López, A.L. Ortiz, Transient liquid-phase assisted spark-plasma sintering and dry sliding wear of B_4C ceramics fabricated from B_4C nanopowders, J. Eur. Ceram. Soc. 41 (3) (2021) 1869–1877.
[18] C. Ojalvo, R. Moreno, F. Guiberteau, A.L. Ortiz, Processing of orthotropic and isotropic superhard B_4C composites reinforced with reduced graphene oxide, J. Eur. Ceram. Soc. 40 (9) (2020) 3406–3413.
[19] C. Ojalvo, R. Moreno, F. Guiberteau, A.L. Ortiz, Pressureless ultrafast sintering of near-net-shaped superhard isotropic B_4C/rGO composites with Ti-Al additives, J. Eur. Ceram. Soc. 40 (12) (2020) 4354–4360.
[20] C. Ojalvo, M. Ayllón, A.L. Ortiz, R. Moreno, Aqueous tape casting of super-hard B_4C laminates with rGO-enriched reinforcing interlayers, J. Eur. Ceram. Soc. 41 (11) (2021) 5457–5465.
[21] R.E. Mistler, E.R. Twiname, Tape Casting: Theory and Practice, Wiley, 2000.
[22] Y.Q. Li, T. Qiu, Oxidation behaviour of boron carbide powder, Mat. Sci. Eng. A 444 (2007) 184–191.
[23] M. Barsoum, Fundamentals of Ceramics, McGraw-Hill, New York, 1997.
[24] R.M. German, Sintering Theory and Practice, Wiley, New York, 1996.